NUREG/CR-2317
BNL-NUREG-51419
VOL. 2, NO. 1

CONTAINER ASSESSMENT — CORROSION STUDY OF HLW CONTAINER MATERIALS

QUARTERLY PROGRESS REPORT
JANUARY - MARCH 1982

T.M. Ahn and P. Soo

Date Published - June 1982

NUCLEAR WASTE MANAGEMENT DIVISION
DEPARTMENT OF NUCLEAR ENERGY, BROOKHAVEN NATIONAL LABORATORY
UPTON, LONG ISLAND, NEW YORK 11973

Prepared for the U.S. Nuclear Regulatory Commission
Office of Nuclear Regulatory Research
Washington, D.C. 20555

NUREG/CR-2317
BNL-NUREG-51449
VOL. 2 NO. 1
AN, WH

CONTAINER ASSESSMENT — CORROSION STUDY OF HLW CONTAINER MATERIALS

QUARTERLY PROGRESS REPORT JANUARY - MARCH 1982

T.M. Ahn and P. Soo
Principal Investigators

Contributors:
B.S. Lee
J. Woodward
R. Sabatini

Manuscript Completed — April 1982
Date Published — June 1982

Prepared by
NUCLEAR WASTE MANAGEMENT DIVISION
D.G. SCHWEITZER, HEAD
DEPARTMENT OF NUCLEAR ENERGY
BROOKHAVEN NATIONAL LABORATORY
ASSOCIATED UNIVERSITIES, INC.
UPTON, LONG ISLAND, NEW YORK 11973

PREPARED FOR THE U.S. NUCLEAR REGULATORY COMMISSION
OFFICE OF NUCLEAR REGULATORY RESEARCH
CONTRACT NO. DE-AC02-76CH00016
FIN NO. A-3237

ABSTRACT

Crevice corrosion products formed on titanium base materials exposed to WIPP Brine A at 150°C have been analyzed by obtaining electron diffraction patterns of oxide films which were selected from various positions on the crevice surface. The crevice corrosion products for CP titanium and TiCode-12 are mainly an anatase form of TiO_2. Both materials also showed trace amounts of Ti_3O_5. The intensity of the Ti_3O_5 peak in the diffraction pattern is stronger in CP titanium than in TiCode-12. More Ti_3O_5 is formed in the center of the crevice. From the study, it seems that the color differences of oxides inside the crevice are mainly due to optical interference colors caused by varying film thickness.

The open-circuit corrosion potential behavior of CP titanium and TiCode-12 has been examined in acidified Brine A at 80°C. To reduce the potential effect of oxidizing impurities in test media these solutions were pre-electrolyzed. Both materials show breakdown of the passive film. TiCode-12 reaches a quasi steady state potential more rapidly than CP titanium. Breakdown of the passive film is attributed to the high chloride concentration with Ni being preferentially dissolved.

Single-edged-notched tensile specimens have been used to obtain the apparent stress intensity factors at 2% crack extension in hydrogenated TiCode-12 with hydrogen concentrations up to 10,900 ppm. For high hydrogen levels the apparent stress intensity factor dropped roughly by a factor of 10 compared to nonhydrogenated TiCode-12. Fractographs show both alpha phase crystallographic fracture and alpha-beta interface cracking. These fractographs indicate that the formation of hydride is responsible for crack initiation for hydrogen concentrations above 5000 ppm.

Notched c-rings of CP titanium and TiCode-12 have been loaded and immersed in acidified Brine A to test for stress corrosion cracking susceptibility. These tests are presently under way.

CONTENTS

FIGURES

FIGURES (Continued)

ACKNOWLEDGMENT

Our thanks go to G. Spira and R. Jones for their general technical assistance and P. Klotz and J. Forrest for their work on chemical analyses. We wish to express our sincere appreciation to Ms. S. M. Mcore and Ms. G. F. Searles for their efforts and patience in the typing and preparation of this report.

1. INTRODUCTION

The current program was initiated to determine potential corrosion failure modes in TiCode-12 high level waste container material exposed to prototypic repository conditions. A basic goal was to elucidate the mechanism by which failure occurs and to develop means of extrapolating short term test data to the prediction of very long term container behavior. Work to date in this program has shown that crevice corrosion is a possible failure mode in TiCode-12. This is the first observation that has been made of this type of corrosion in a simulated repository brine environment. Thus, a major part of the BNL effort is directed to finding conditions under which it occurs, determining the precise mechanism of failure, and to evaluating whether the occurence of long term crevice attack will compromise container integrity. Efforts in this quarter have been concentrated on the crevice corrosion and hydrogen embrittlement of TiCode-12 and CP titanium. Electrochemical work in acidified brines has also been performed to aid in understanding the corrosion of these materials in the crevice environment.

2. CREVICE CORROSION

2.1 Identification of the Crevice Corrosion Product

As reported earlier by BNL,[1] it was possible to identify the corrosion product formed in the crevices of TiCode-12 and CP titanium with an electron diffraction technique utilizing TEM (Transmission Electron Microscopy). In this quarter, more work was conducted to obtain additional data for identifying the corrosion products. In the current work, the TEM diffraction samples were selected from different colored parts of the film inside the crevice. This enabled us to study crevice corrosion as a function of the distance from the crevice perimeter and to determine whether the colors are caused by optical interference or by different oxide phases.

2.1.1 TiCode-12

As shown in Figure 1, three samples taken from films with different colors were prepared. The yellow film (position 1, Figure 1) showed crystals with different shapes including pointed and block shaped crystals (Figure 2). All the diffraction rings for the crystals match the peaks for the anatase form of TiO_2, except one peak at d = 1.76Å.

The violet film (position 2, Figure 1) showed mostly block shaped crystals with a few pointed crystals. The diffraction patterns show strong anatase (TiO_2) peaks, with two extra weak peaks at $d \simeq 2.13$ and 1.75Å. Figure 3 is an SEM (Scanning Electron Microscopy) photomicrograph of this violet film.

The blue film (position 3, Figure 1) consisted mostly of block shaped crystals with almost no pointed crystals, as shown in Figure 4. All the strong peaks were identified as those from anatase (TiO_2). Additional peaks ($d \simeq 2.85$, 2.15, 2.03, 1.77, and 1.41Å) were observed although they were very weak.

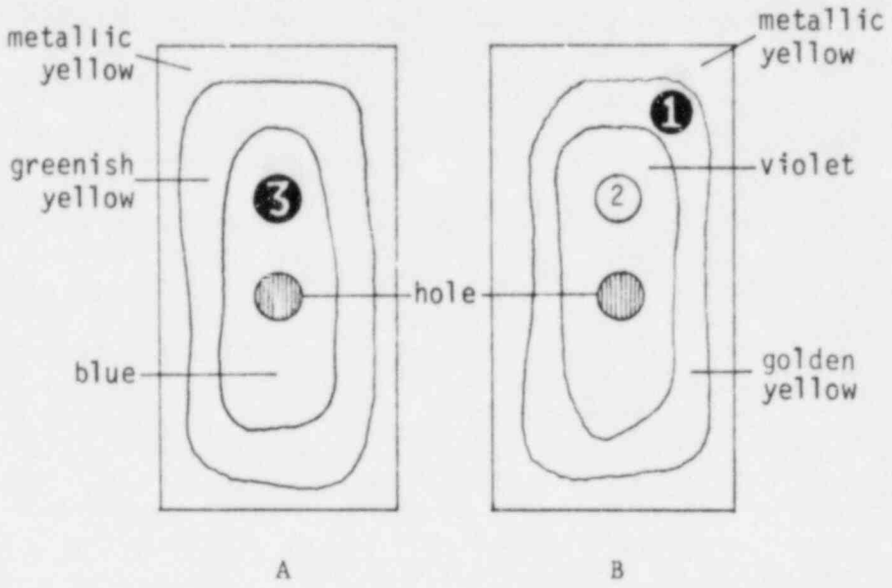

Figure 1. TiCode-12 specimens from which TEM samples were prepared. 1, 2, and 3 denote the locations of the areas studied. Surfaces A and B faced each other to form the crevice. The crevice specimen was immersed in Brine A at 150°C for 24 days.

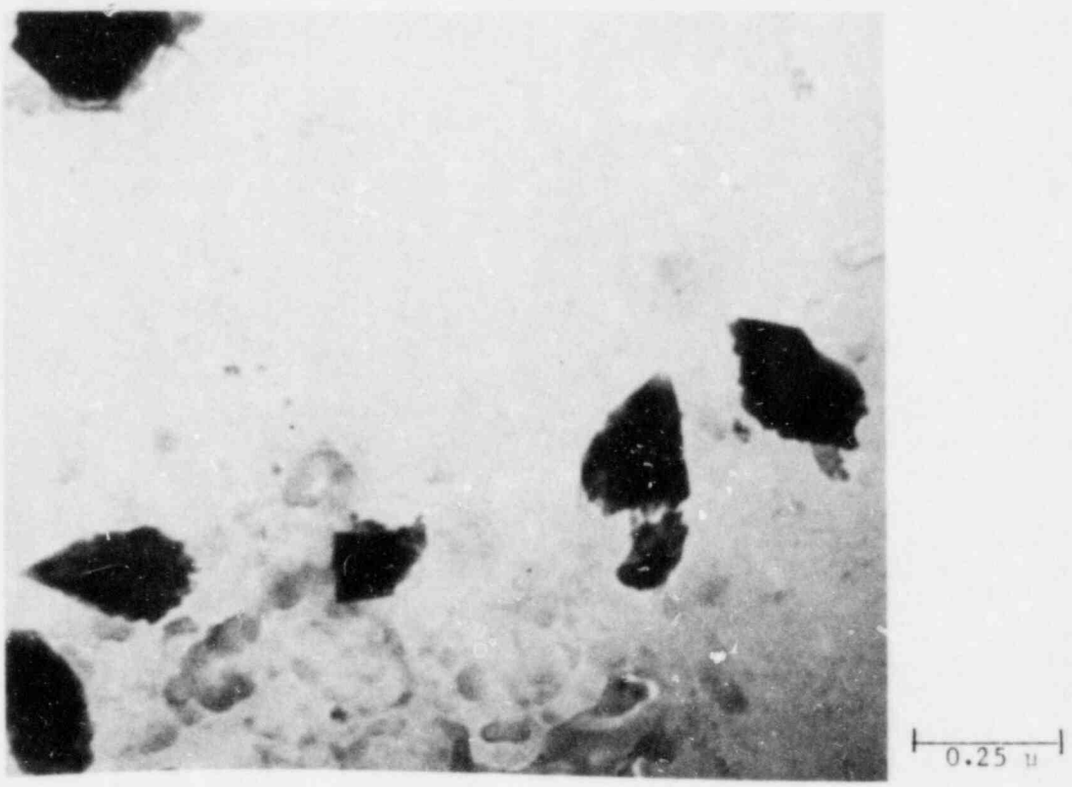

Figure 2. The TEM microstructure of the yellow film formed in position 1 showing pointed and block-shaped crystals.

Figure 3. SEM photomicrograph of the violet film formed inside the crevice of TiCode-12.

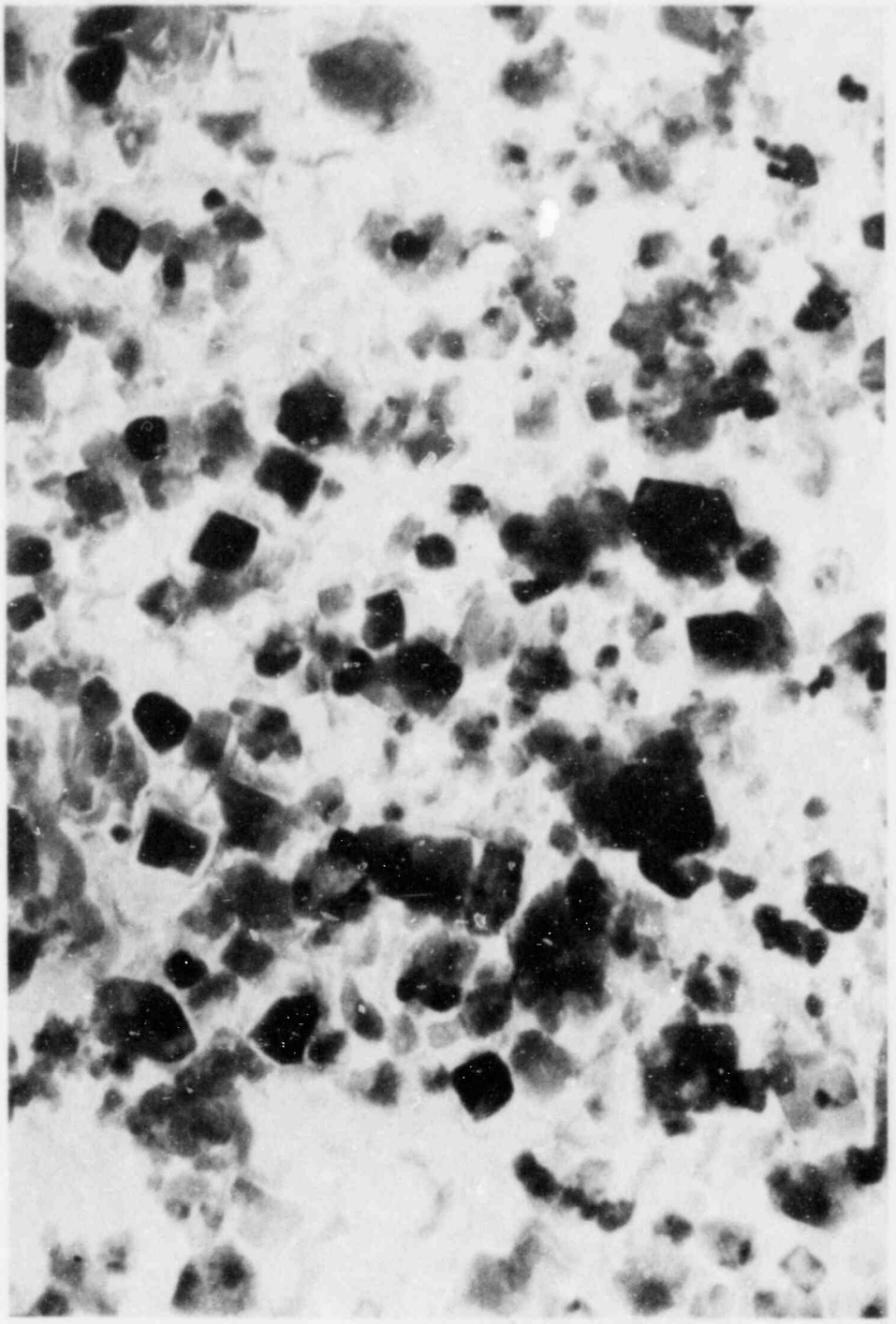

Figure 4. The TEM microstructure of the blue film formed inside the crevice of TiCode-12.

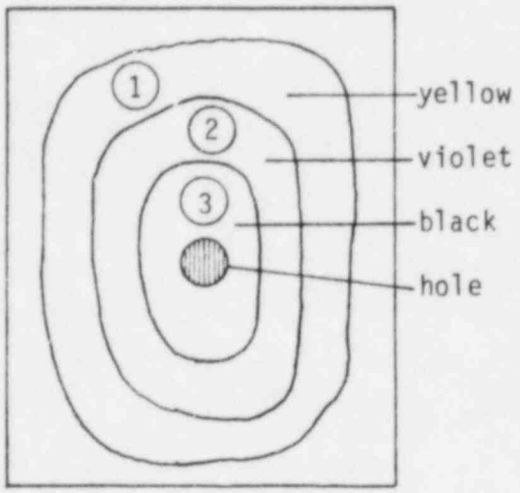

Figure 5. CP titanium crevice corrosion specimen from which TEM samples were prepared. 1, 2, and 3 denote the locations of the areas studied. The crevice specimen was immersed in Brine A at 150°C for 12 weeks.

2.1.2 CP Titanium

As shown in Figure 5, three samples with different colors were prepared from crevice regions. The yellow film (position 1, Figure 5) shows all the diffraction peaks of anatase with one very weak peak at d = 1.75Å. The crystals do not have definite shapes, but are aggregates of small crystallites.

The diffraction pattern of the violet film showed all the peaks expected for anatase. The additional peaks were much stronger than those from TiCode-12 samples, and were more numerous. Figure 6 shows a carbon replica of the anatase crystals.

The black film shows strong extra peaks in addition to anatase peaks, at d ~ 4.49, 2.91, 2.78 (band), 2.16, 1.76, and 1.42Å. It was found that all the extra peaks for the TiCode-12 samples are in fact part of this set for CP titanium. This extra peak set matched best the Ti_3O_5 diffraction pattern.

To compare the difference between the oxides present in the crevices and an air-formed oxide, an oxide film was formed in air on CP titanium using a gas flame. Electron diffraction patterns obtained from this film accurately matched those of the rutile form of TiO_2. The electron diffraction patterns from the crevice corrosion product and the air-formed oxide film are compared in Figures 7a and 7b. The two patterns are distinctly different. It is interesting to note that there was no trace of the rutile form of TiO_2 inside the crevices of CP titanium or TiCode-12 exposed to brine.

Figure 6. Carbon replica of an anatase form of TiO_2 formed inside the crevice of CP titanium.

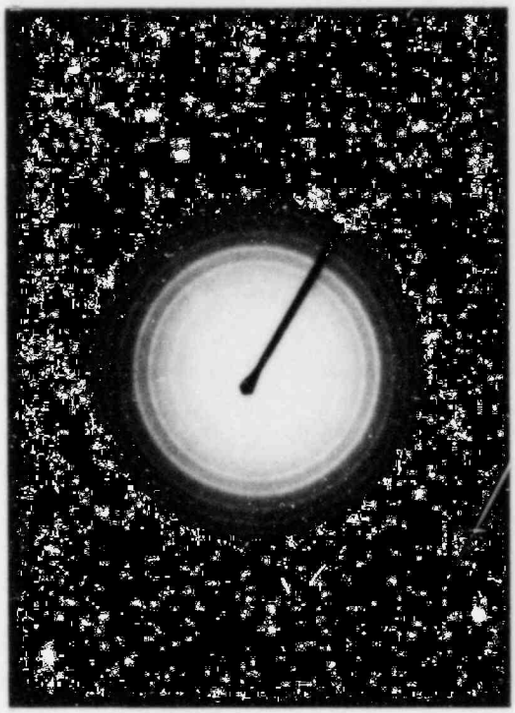

Figure 7a. Electron diffraction pattern from the violet film inside the TiCode-12 crevice.

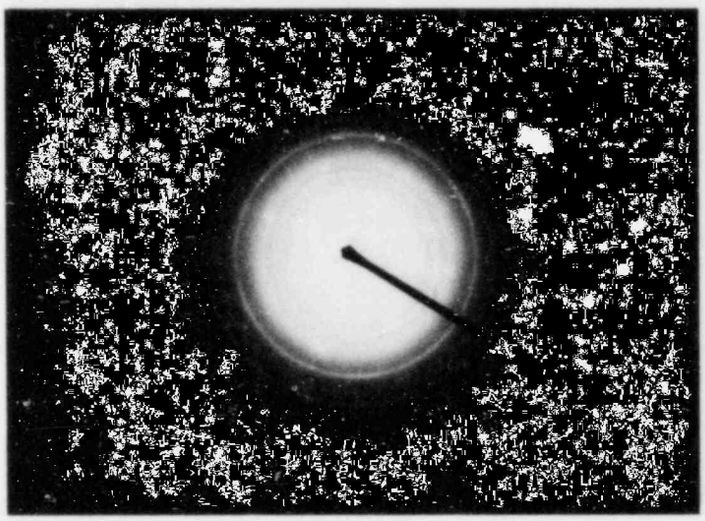

Figure 7b. Electron diffraction pattern from the blue film formed on CP titanium by gas flame oxidation in air.

X-ray diffraction was also used to identify the crevice corrosion product. Because of the small amount of the corrosion product, only one peak was obtained as shown in Figure 8. However, this clearly matches the major peak of the anatase form of TiO_2 (d = 3.52Å).

2.1.3 Summary and Discussion

It can be concluded that the crevice corrosion products formed on CP titanium and TiCode-12 are mainly the anatase form of TiO_2. Both CP titanium and TiCode-12 samples also showed peaks for Ti_3O_5. The intensity of the Ti_3O_5 peaks are stronger in CP titanium than in TiCode-12. It also appears that the greater the distance from the crevice perimeter, the greater the Ti_3O_5 concentration. In addition, optical interference in differing thickness corrosion films can account for the observed colors of these films.

In the literature, three different oxide forms have been reported as possible corrosion products of titanium and its alloys in acidic solutions[2,3] or in neutral NaCl solutions.[4,5] These are stable rutile forms of TiO_2 (tetragonal crystal structure), the metastable anatase form of TiO_2 (tetragonal crystal structure) and another metastable brookite form of TiO_2 (orthorhombic crystal sructure). Metastable forms have been reported to be responsible for passivation,[2] i.e., the formation of surface films which drastically slow down corrosion processes. On the other hand, the rutile form is known to be porous and it appears quite often adjacent to the metastable form and near to the solution, or as a result of precipitation of the dissolved metal ions. Also, air formed titanium oxide has been shown to be rutile.[3] However, there have been no comprehensive studies in the literature on the identification of oxide films formed in various environments using surface sensitive analytical techniques.

Our present findings regarding the types of films are quite different to those stated above. This may be a result of the new brine environment used in this work. The existence of lower oxides suggests that a potential distribution exists inside the crevices. The major questions remaining to be answered are: (1) are these oxides barriers to corrosion? and (2) are these oxide hydrolysis products as a result of continuous metal dissolution? Work is continuing to obtain answers to these questions.

2.2 The Effects of Surface Oxidation State on the Crevice Corrosion of TiCode-12

The outer surfaces of TiCode-12 crevice samples (2 cm x 2 cm) were oxidized in air using a gas flame, and immersed in a Brine A solution at 150°C for 24 days. This preoxidation of the outer surface is a method of varying the cathodic reaction rate during crevice corrosion. The sample showed black colored corrosion products inside the crevice, while regularly finished samples usually showed violet/blue films in this region. This indicates that the rate of cathodic reaction probably changes the corrosion potential and/or the solution chemistry inside the crevice. The corrosion products will be analyzed to evaluate this effect.

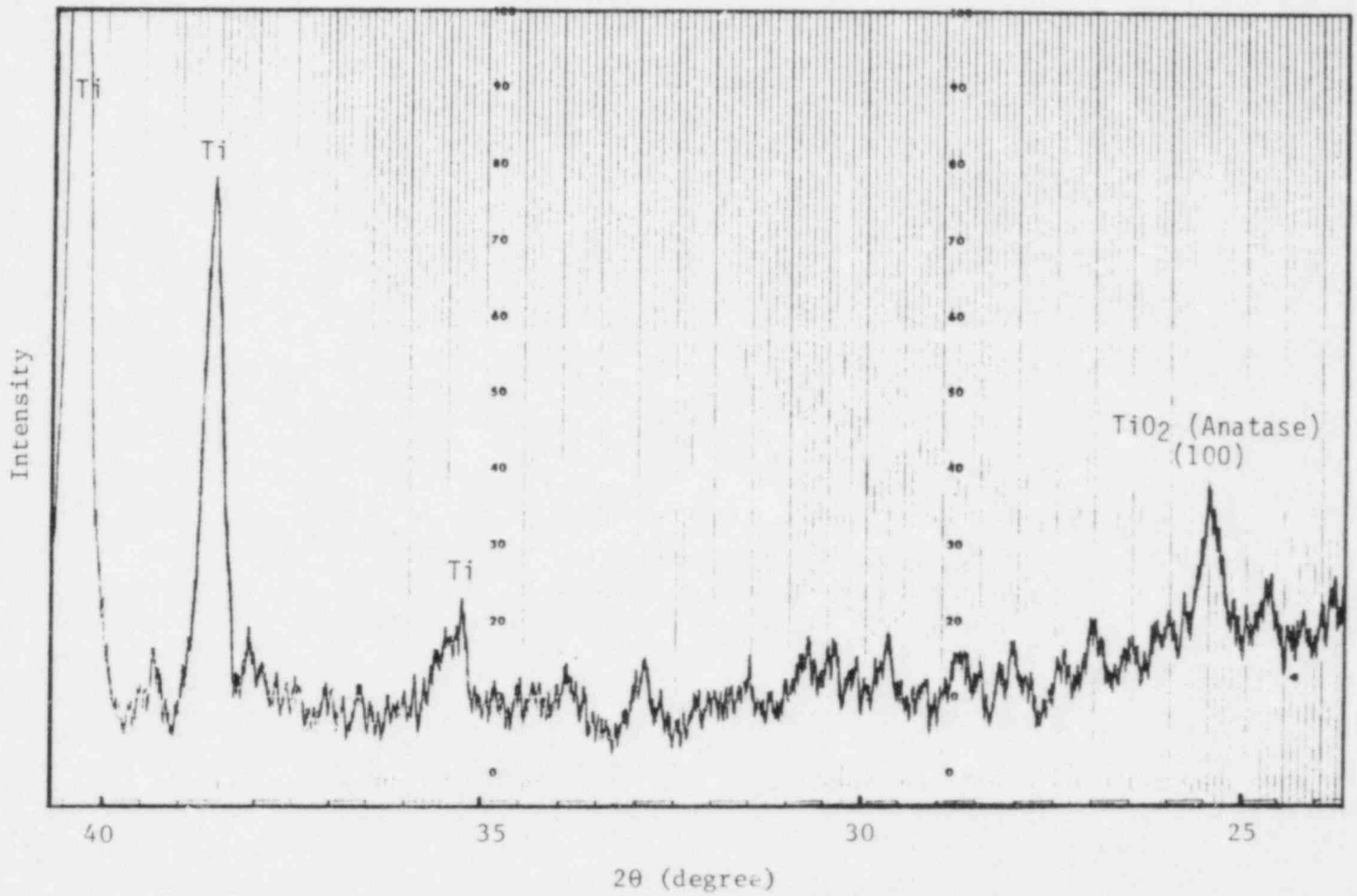

Figure 8. X-ray diffraction pattern of the crevice corrosion product of CP titanium.

3. ELECTROCHEMISTRY

Acidified brine is expected to form in a titanium crevice environment. In order to obtain kinetic data on the effect of acidified brine on the passivation behavior of unalloyed titanium and TiCode-12, the open circuit (o/c) potential behavior of both was examined at 80°C. An electrochemical cell with a rotating disc electrode (defined mass transport) and a special gas scrubber system enabling solution oxygen levels of approximately 1 ppb was used. The saturated calomel reference electrode used was placed directly in the hot brine. It was noted that the analytical reagents used in making up the brine contained trace impurities considered capable of influencing the redox potential of the solution, e.g., Fe^{+3} and NO_3^-. By pre-electrolyzing the solution, i.e., by electrochemically reducing the impurity species to a lower oxidation state, a redox potential of the brine solution would be obtained which is closer to that expected from the ionic concentrations. Following pre-electrolysis of the solution, specimens of CP titanium and TiCode-12 polished (with 600-grit SiC paper) and ultrasonically cleaned (in distilled H_2O) were anodized for five minutes at a potential of +200 mV sce, to minimize the influence of the thickness of the air formed oxide film. Potentiostatic polarization was discontinued and immediately the potential became less noble (more cathodic) in both cases. In the case of CP titanium, the potential fell instantly to ~-120 mV sce (Figure 9) and for TiCode-12 the potential attained a value of ~-360 mV sce (Figure 10). After approximately four hours immersion, the potential of the TiCode-12 specimen reached a value of ~-550 mV sce. The corresponding time for the CP titanium specimen to reach the same potential was ~14 hours. However, the o/c potential of the TiCode-12 specimen did not change appreciably (i.e., -550 to -530 mV sce) at termination of the test at ~20 hours total immersion time. In contrast, the o/c potential of the CP titanium specimen continued to fall until its potential was essentially constant with E ~-620 mV sce at a time of ~17 hours. In the process of attaining an essentially steady state condition, both materials exhibited evidence of potential excursions (Figures 9 and 10).

An attempt was made to determine the corrosion rate (anodic dissolution rate) of the TiCode-12 specimen using an ac polarization technique. To a first approximation, the current density was determined to be 5 $\mu A\ cm^{-2}$ after 24 hours' immersion. If this rate remained constant it would indicate that in 1000 years the depth of metal penetrated could be ~100 mm in an acidic medium containing high halide concentrations. It must be assumed, however, that as the crevice becomes larger the rate of dissolution would decrease since true crevice conditions would disappear.

Previous investigators[4,5] of the behavior of Ti in acidified chloride solutions consider that Ti is passive at potentials greater than ~-300 mV sce at pH = 1 and for a chloride concentration $[Cl^-]$ equal to 1 M. The chloride concentration in the present acidified Brine A is equivalent to a molarity of ~5.35 M. According to Griess[4] the chloride ion concentration is of lesser importance than the hydrogen ion activity. However, Griess does consider that the actual salt concentration is important, i.e., the more concentrated the salt, the more severe the attack, irrespective of the halide ion. Based on

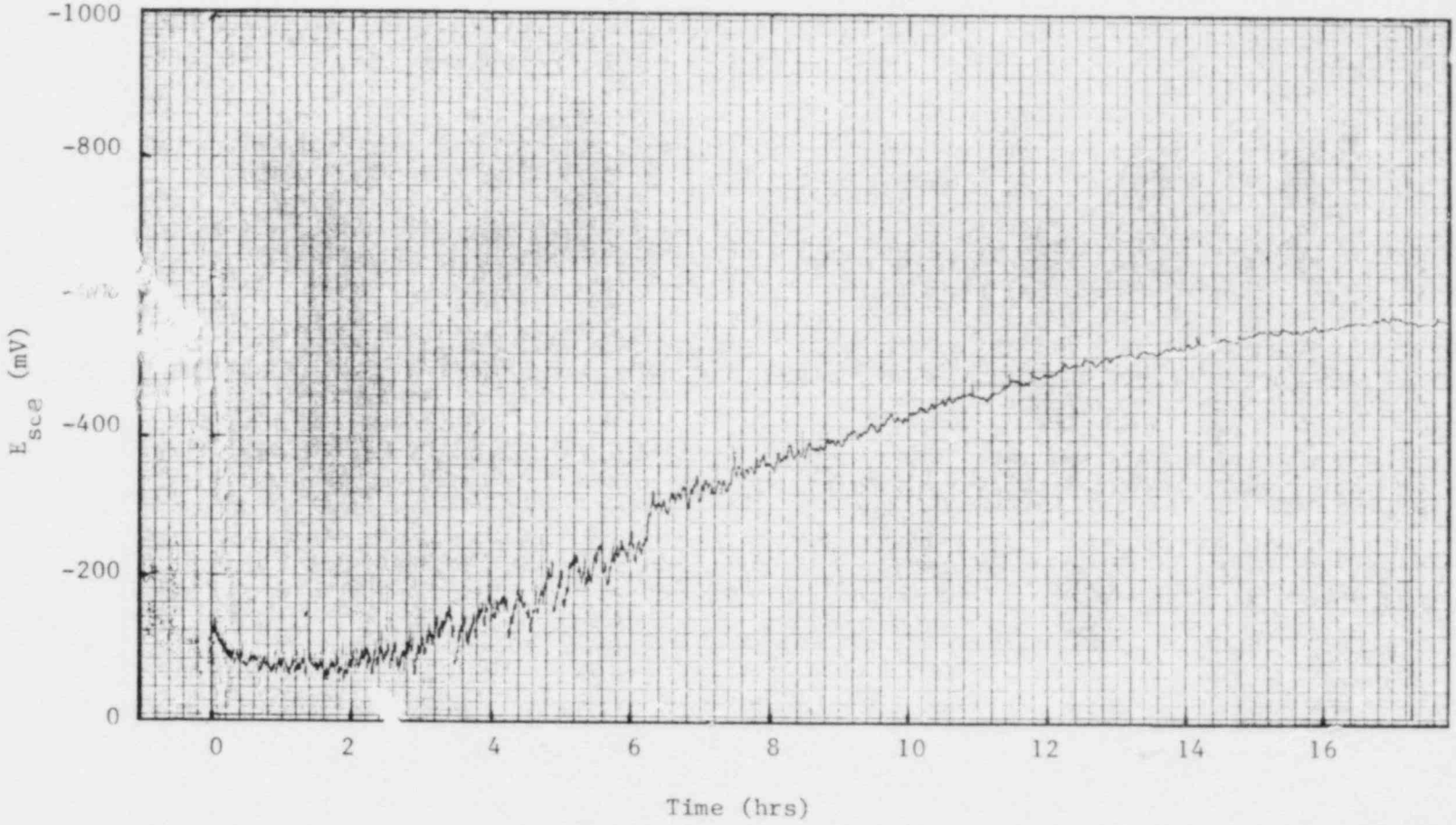

Figure 9. Open-circuit corrosion potential of CP titanium in acidified Brine A at 80°C.

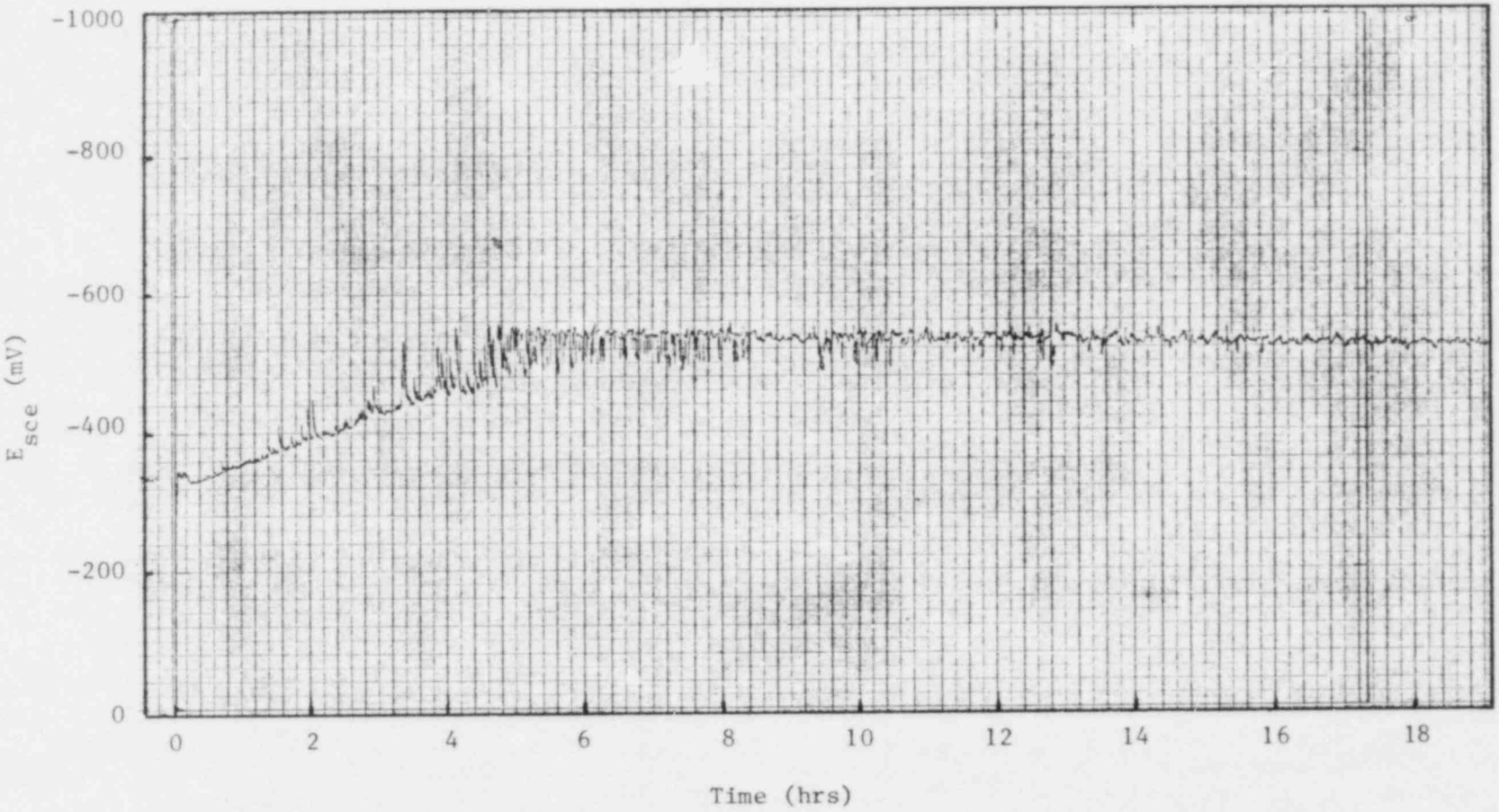

Figure 10. Open-circuit corrosion potential of TiCode-12 in acidified Brine A at 80°C.

Kelly's model[6] whereby passivation of an active surface is achieved by attaining some critical concentration of Ti(IV) ions, the present results for titanium in acidified brine could be considered in terms of a higher chloride/halide concentration necessitating a higher concentration of Ti(IV) ions to be present in solution before the surface is passivated.

The free corrosion potential of CP titanium suggests that it was initially in a passive state (E ~-120 mV sce, Figure 9) whereas TiCode-12 was not (E ~-340 mV sce, Figure 10). After approximately two-hours' immersion the passive behavior of the CP titanium surface appears to change in that the potential became more cathodic and fluctuated until E was ~-300 mV sce (Figure 9). The fluctuations probably indicate the ability of bulk impurities in the metal (e.g., Fe) surface to maintain passivation, but which are themselves cyclically depleted and enriched in the surface by dissolution. As film breakdown continues, the facility with which the bulk impurities can maintain passivation is reduced and the potential continues to fall until E ~-300 mV sce. In this potential range, the oxide film is reduced to a monolayer, according to Kelly.[6] The rapid decrease in potential at this point reported for high purity titanium (pH = 0, $[Cl^-]$ = 1 M) by Kelly[6] is not observed here and may be due to the continued influence of the bulk impurities.

With continued immersion, the potential decreased linearly at an approximate rate of 34 mV per hour. After about 17 hours, it reached a "steady state" value of E ~-620 mV sce. This potential is similar to the open circuit potential attained by CP titanium under similar conditions following mechanical removal of the oxide (allowing for the difference in $[Cl^{-1}]$).[1] In fact, this potential ~-620 mV sce is very close to the potential shown by both Griess[4] and Kelly[6] at pH = 1 and $[Cl^-]$ = 1 M to be that associated with the maximum corrosion rate and is independent of temperature.

The observations for TiCode-12 require further analysis. Previously it was reported that for similar conditions but lower Cl^- concentration ($[Cl^-]$ = 1 M) an abraded TiCode-12 surface attained a potential of approximately -400 mV sce after approximately 83 minutes.[1] After the same time the o/c potential of TiCode-12 in acidified brine reaches approximately the same potential but at this point fluctuations in the potential are noted (Figure 10). It is not considered that these fluctuations are due to the same source (i.e., bulk impurities such as Fe) as in the case of CP titanium since the potential is considerably more cathodic and the fluctuations are much more rapid. Reference to work by Griess[4] reveals that a Ti-1% Ni-1% Mo alloy also exhibited essentially similar potential cycling over a time period of approximately 20 minutes. In this work, the time period was an order of magnitude shorter. Also, the fluctuation ranges from -315 mV sce to -470 mV sce in Griess'[4] work while the present study shows the average fluctuations varied from -550 mV sce to -480 mV sce, i.e., remaining more or less active. Reference to thermodynamic data allows some pertinent comments to be made regarding this fluctuation behavior of TiCode-12. In the potential range covered by the fluctuations, dissolution of Mo could be expected to be appreciably less than in the case of Ni, after considering the Pourbaix diagrams for Ni and Mo.[7] Further, in the case of stainless steel containing Mo, the mechanism of crevice corrosion inhibition in acidic chloride environments is

most probably associated with the formation of insoluble MoO_2 which reduces active dissolution.[8] Hence, it is highly likely that the observed oscillatory potential behavior is a result of varying concentrations of Ni at the surface as a result of the dissolution. After some time, there should be an appreciable buildup of Mo on the surface, reducing the influence of the Ni concentration on the surface behavior. This is illustrated in Figure 10, which shows much smaller potential fluctuations, ~15 mV, after approximately eight hours. A buildup of Mo in the surface film would then be responsible for the "steady state" corrosion potential observed after ~18 hours.

These results are preliminary. Nevertheless, it can be concluded that the breakdown of the passive film on TiCode-12 in the presence of acidified Brine A is most probably due to the dissolution of Ni as a result of the high halide concentrations used. Continuing efforts will be made to explore this behavior further at higher temperatures and with various halides and oxidant ion concentrations.

4. HYDROGEN EMBRITTLEMENT

Up to this time,[1] the fractographic analysis of hydrogenated TiCode-12 has been performed on smooth tensile specimens without notches. In this quarter, fracture mechanics samples were used to control the crack path and define the stress intensity level. Single-edged-notched tensile specimens, 15 x 2 x 10 cm with a 45 degree notch extending to a depth of 3 mm, were machined in the samples. The surface was finished to 600-grit SiC. Prior to testing, a fatigue crack approximately 0.5-mm long was introduced at the notch in the specimens. The hydrogenation of the samples was performed by heat treating the samples in a vacuum furnace, backfilled with ultra high purity hydrogen. Before the backfilling, the furnace was evacuated to 10^{-7} torr. The heat treating time was 750°C for five hours at vacuum, and 190 and 760 torr of hydrogen. The specimens were tension tested to failure at a crosshead speed of 0.005 cm/min. The apparent stress intensity factor at 2% crack extension, K_Q, was estimated from the force-displacement curves following the ASTM procedure[9] using the formula given by Srawley and Brown[10]. This calculation is an estimate since the Poisson ratio of hydrogenated TiCode-12 has not been measured and there is a potential problem of crack blunting in the fatigue precracking process. Currently, these problems are being resolved. After testing, the fracture surface was examined in an SEM and a vacuum extraction method was used to determine the hydrogen concentration.

Table 1 shows the approximate K_Q values and hydrogen concentration levels of the tested samples. At a 100-ppm hydrogen concentration, the sample was very ductile with a slanted fracture surface[11] suggesting that plane strain conditions had not been achieved for this thickness. The fracture surface is very ductile with dimples as shown in Figure 11.

The hydrogen backfill pressures of 190 and 760 torr both gave hydrogen concentrations above 5000 ppm. The K_Q values do not show a systematic trend as shown in Table 1. However, the K_Q values for the 6560 or 10900-ppm hydrogen samples differ within experimental error. At these levels of

Table 1

The Apparent Stress Intensity Factor at Crack Initiation at Three Hydrogen Concentration Levels

Hydrogen Concentration (ppm)	100	6560	10900
K_Q (MPa $\sqrt{m}$)	45.4	4.5	5.8

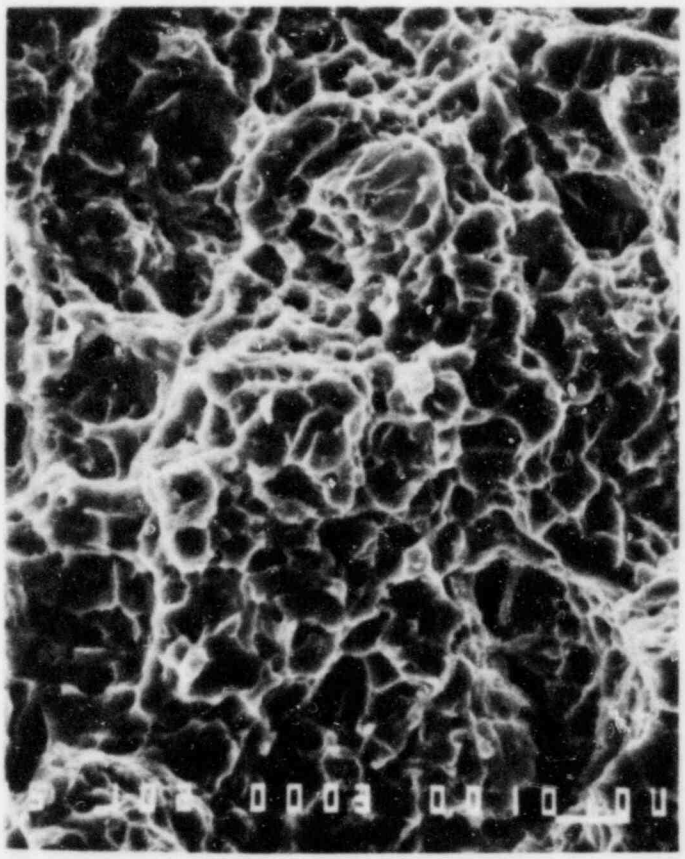

10 μ

Figure 11. Ductile fracture of TiCode-12 with a hydrogen concentration of 100 ppm.

hydrogen concentration, the samples have become brittle showing no slanted fracture surfaces. The stress level needed for crack growth is apparently sufficiently low to obtain plane strain conditions. The observed sharp drop in force in the force-displacement curve may indicate that K_Q values obtained approximate the true threshold stress intensity factor K_{th} (stress intensity factor at crack initiation). Currently, the testing is being repeated at lower and higher hydrogen concentrations using partial unloading techniques.[12]

The fractographs obtained for high hydrogen concentrations show both alpha phase cleavage and interface cracking. Figure 12 shows a typical example of an interface crack showing surface facets. When the sample is rotated, the facets may be examined more easily as shown in Figure 13. This figure is quite similar to the fractographs observed in other near-alpha titanium alloys.[13] Figure 14 shows intermittent crack propagation in a grain and a secondary interface crack developed in the center of the microcrack. The grain size is much smaller than the figure size indicating that the fracture mode is alpha phase cleavage. The direction of intermittent crack propagation changes depending on the grain orientation. Also, at least two different orientations of crack propagation in one grain are observed. This suggests crystallographic fracture in the alpha grain as discussed by other authors.[14] Figures 15 and 16 show quite clearly this crystallographic fracture. Meyn has identified this feature as the cleavage of alpha phase on or near the (0001) basal plane in Ti-6Al-4V.[15] Meyn,[16] and Blackburn and Williams[17] have found the cleavage-like facets lie approximately 14 degrees from (0001). Figure 17 shows another feature of crystallographic fracture. However, in this case, there is a possibility that the cleavage might be from interface cracking since the interface also has crystallographic features.[13] Currently, this crystallographic behavior is being investigated using Laue back-reflection techniques to determine the cleavage surface orientation.

As mentioned above, the fractographic observations in comparison to other near-alpha titanium alloys suggest that hydride formation is probably responsible for the hydrogen embrittlement of TiCode-12 at least at hydrogen concentrations above 5000 ppm. The mechanism may be:

- stress assisted hydride formation at the crack tip and subsequent crack propagation along the matrix-hydride interface;[18] or
- preferential segregation of hydrogen in the beta phase and hydride precipitation at the alpha/beta interface leading to alpha/beta interfacial separation.[19]

In future work quantitative values of K_{th} will be generated as a function of temperature and hydrogen concentration.

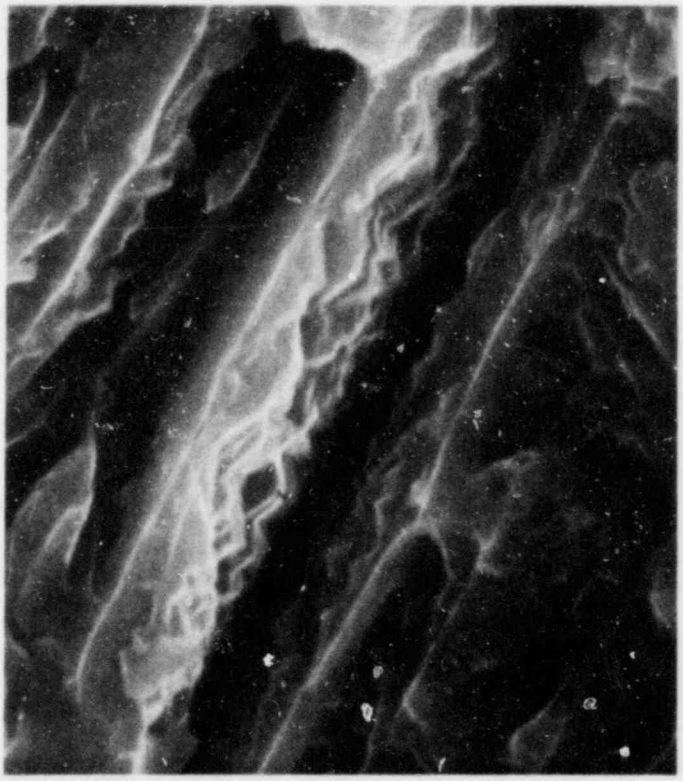

Figure 12. Hydrogen induced interface facets formed by brittle interface cracking of TiCode-12 with hydrogen above 5000-ppm.

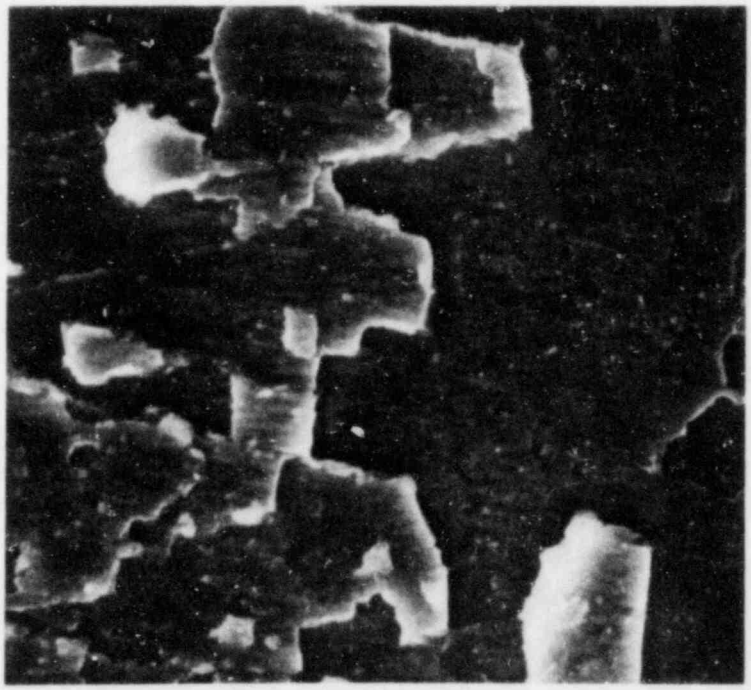

Figure 13. Hydrogen induced interface facets observed after rotation of the sample position in Figure 12.

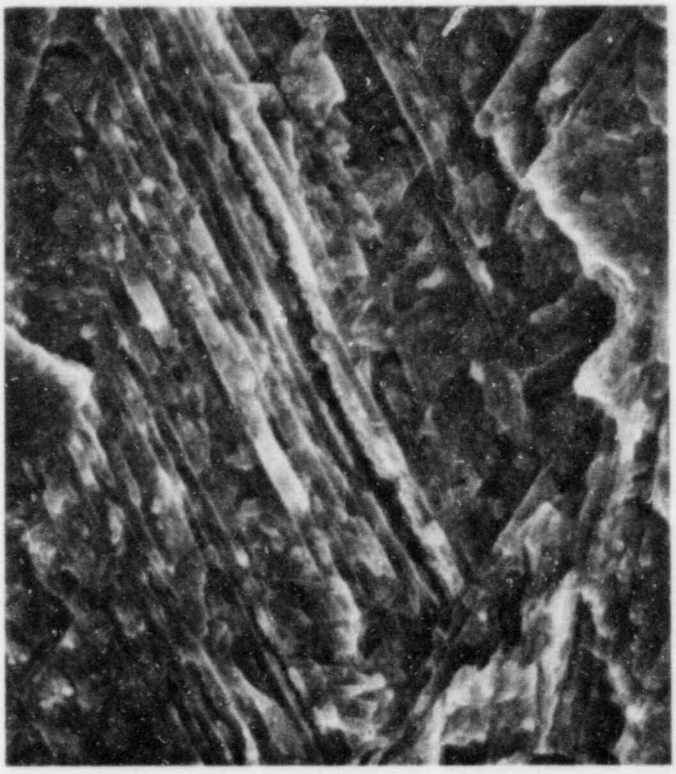

Figure 14. Hydrogen induced intermittent brittle crack propagation in a grain of TiCode-12 with hydrogen concentration above 5000 ppm. Note secondary interface cracking in the center.

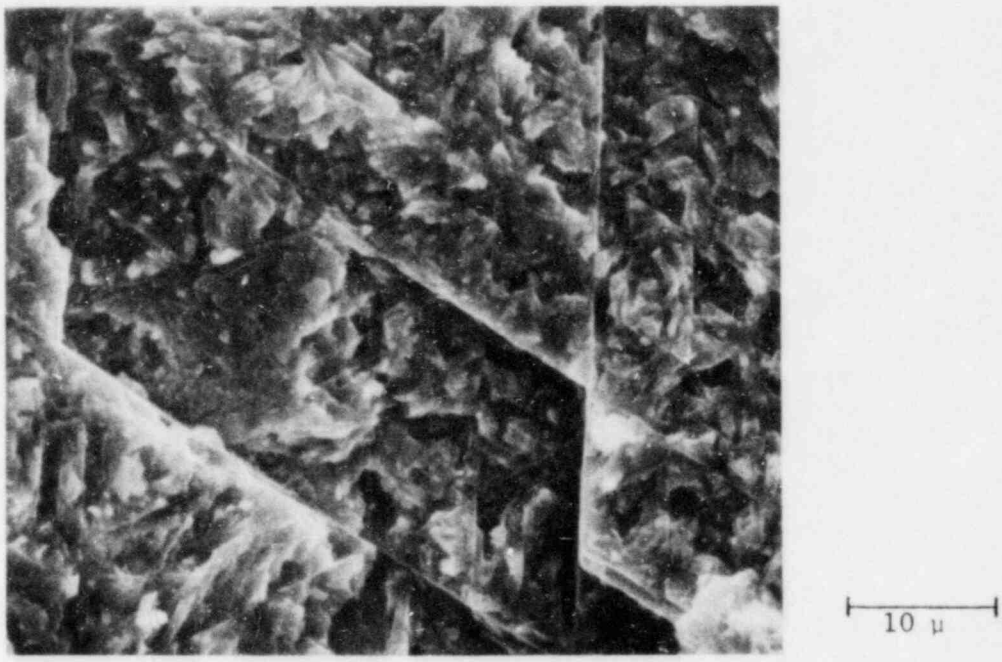

Figure 15. Fracture surface of TiCode-12 with hydrogen concentration above 5000 ppm showing crystallographic fracture, magnification 2000X.

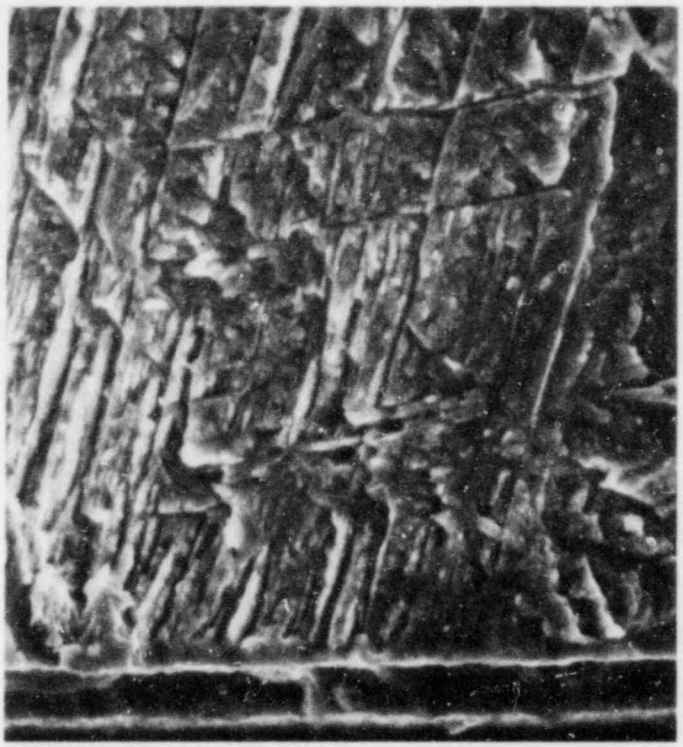

Figure 16. Fracture surface of TiCode-12 with hydrogen concentration above 5000 ppm showing crystallographic fracture, magnification 1000X.

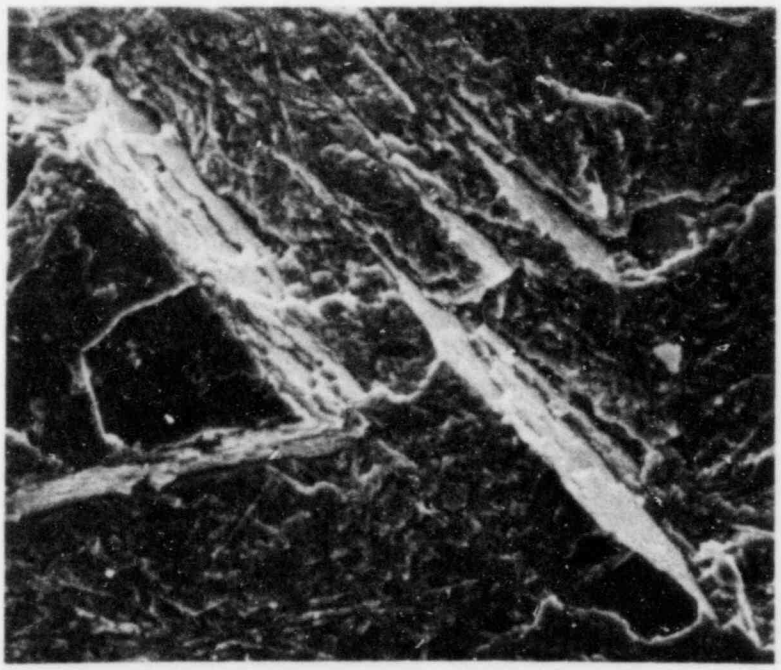

Figure 17. Fracture surface of TiCode-12 with hydrogen concentration above 5000 ppm showing crystallographic fracture, magnification 500X.

5. STRESS CORROSION CRACKING

Notched c-rings of CP titanium and TiCode-12 have been calibrated (using an SR-4 type K strain indicator). Both notched and un-notched c-rings were loaded and sealed in a capsule containing acidified Brine A to simulate crevice corrosion conditions i.e., adjusted to a pH of 1 (volume/surface area ratio approximately 6.5). Notched c-rings of CP titanium and TiCode-12 which were plastically deformed prior to immersion are also being tested. The test temperature is 150°C.

6. REFERENCES

1. T. M. Ahn, P. Soo, et al., "Container Assessment - Corrosion Study of HLW Container Materials, Quarterly Progress Report," July-September 1981, October-December 1981, NUREG/CR-2317, BNL/NUREG-51449, Vol. 1, Nos. 3 and 4, 1982.

2. N. D. Tomashov, G. P. Chernova, Y. S. Ruscol, and G. A. Ayuyan, "The Passivation of Alloys on Titanium Bases," Electrochemica Acta. 19, 159 (1974).

3. T. Koizumi and T. Nakayama, "Structure of Oxide Films Formed on Ti in Boiling Dilute H_2SO_4 and HCl," Corrosion Science 8, 195 (1968).

4. J. C. Griess, Jr., "Crevice Corrosion of Titanium in Aqueous Salt Solutions," Corrosion-NACE 24, 96 (1968).

5. L. L. Shreir, "Localized Corrosion," in Corrosion, Vol. 1, L. L. Shreir, Ed., Newnes-Butterworths, 1979.

6. E. J. Kelly, "Anodic Dissolution and Passivation of Titanium in Acidic Media," J. Electrochemical Soc. 126, 2064 (1979).

7. M. Pourbaix, Atlas of Electrochemical Equilibria in Aqueous Solutions, NACE (1974).

8. J. N. Wanklyn, "The Role of Mo in the Crevice Corrosion of Stainless Steels," Corrosion Science 21, 211 (1981).

9. Standard Test Method for Plane-Strain Fracture Toughness of Metallic Materials, ASTM E399-81 (1981).

10. J. E. Srawley and W. F. Brown, "Fracture Toughness Testing Measurements," Fracture Toughness Testing, p. 190, ASTM STP 381 (1964).

11. J. F. Knott, Fundamentals of Fracture Mechanics, John Wiley and Sons, 1973.

12. Standard Test for J_{1c}, A Measure of Fracture Toughness, ASTM, E813-81 (1981).

13. D. A. Meyn, "Effect of Hydrogen Content on Inert Environment Sustained Load Crack Propagation Mechanisms of Ti-6Al-4V," in Environmental Degradation of Engineering Materials in Aggressive Environments, M. R. Louthan, Jr., R. P. McNitt, and R. D. Sission, Jr., Eds, VPI, Virginia, 1981.

14. G. H. Koch, A. J. Bursle, R. Liu, and E. N. Pugh, "A Comparison of Gaseous Hydrogen Embrittlement, Slow-Strain-Rate Hydrogen Embrittlement, and Stress-Corrosion Cracking in Ti-8Al-1Mo-1V," Met. Trans. A. 12A, 1823 (1981).

15. D. A. Meyn, "Effect of Hydrogen on Fracture and Inert-Environment Sustained Load Cracking Resistance of Alpha-Beta Titanium Alloys," Met. Trans. A. 5, 319 (1974).

16. D. A. Meyn and G. Sandoz, Met. Trans. 245, 1253 (1969).

17. M. J. Blackburn and J. C. Williams, Fundamental Aspects of Stress-Corrosion Cracking, p. 620, NACE, Houston, 1969.

18. N. R. Moody and W. W. Gerberich, "Hydrogen Induced Slow Crack Growth in Ti-6Al-6V-2Sn," Met. Trans. A 11A, 973 (1980).

19. D. A. Meyn, paper presented at TMS-AIME Fall Meeting in Niagara Falls, New York, September 1976.

120555051503 1 ANRW
US NRC
ADM DIV OF TIDC
PAT LARKINS
LA 212
WASHINGTON DC 20555